JOURNAL OF ENGINEERING AND TECHNOLOGY, Vol. 10 No. 1 June 2012 ISSN 1684-4114
http://www.iutoic-dhaka.edu/jet

A THEORITICAL INVESTIGATION OF TORQUE AND DRAG CHARACTERISTICS OF A SIX BLADED SAVONIUS ROTOR

Shamsun Nahar*, Md. Quamrul Islam* and **Mohammad Ali***

Received 08 March 2012; Accepted after revision 30 June 2012

ABSTRACT

The research work has been carried out to study the aerodynamic characteristic i.e., drag coefficient torque coefficient etc. of a vertical axis type six bladed Savonius rotor. At first drag and torque characteristics of the six bladed Savonius rotor are determined by measuring the pressure distribution over the convex and concave surfaces of each blade at different angle of rotation. The experiment has been carried out at a Reynolds number of 2×10^5 in a uniform flow jet produced by an open circuit wind tunnel. The pressure measurements have been made at 13 tapping points on each two blades of the rotor. Pressure on the convex and concave surfaces have been measured for every 10° interval of rotor angle up to 360° angle of rotation. The data obtained experimentally has been presented in terms of non-dimensional coefficients. To calculate drag force and torque in non-dimensional form, computer based software has been used and the output has been subsequently plotted and analyzed. The effects of individual blade and also the combined effects of six blades on different aerodynamic characteristics are analyzed in this research work. A quasi-steady approach has been applied for the

* *Department of ME, Bangladesh University of Engineering and Technology (BUET), Dhaka-1000, Bangladesh. Email: nahar_306@yahoo.com*

prediction of the dynamic performance of the rotor using the static drag and torque coefficients. Power coefficient versus tip speed ratio curve for six bladed Savonius rotor has been drawn. This method results in a reasonable agreement with the measured power coefficient.

Keywords: *Drag Coefficient, Torque Coefficient, Wind Turbines, Tip Speed Ratio, Wind Power.*

1 INTRODUCTION

The science of exploitation of wind power is not a new one. For the past few centuries people are extracting energy from the wind in various ways. One means for converting wind energy to a more useful form is through the use of windmills. Recently, due to the fuel crisis, this science is gaining more popularity. Wind energy has become very lucrative now-a-days due to its reliability. The European Wind Energy Association (EWEA) estimates that between, 20 GW and 40 GW of offshore wind energy capacity will be operating in the European Union by 2020. A fully developed European offshore wind resources could deliver a capacity of several hundred GW which shows keen interest to develop efficient and economic devices to collect energy from the wind. Recently, the utilization of wind power is increasing in many developed as well as under developed countries. There are various types of windmills. The most common one having the blades of airfoil shape is the horizontal axis wind turbine. Another type is the vertical axis wind turbine with the simplicity of its manufacture compared to horizontal axis wind turbine. Among the different vertical axis wind turbines, the Savonius rotor is a slow running wind machine and has a relatively lower efficiency. Still it is being used in the developing countries because of its simple design, easy and cheap technology for construction and a good starting torque, independent of wind direction and starts at low wind speeds [1, 2, 3]. Rigorous studies on the performance characteristics of the Savonius rotor are found in the literatures and these enable the identification of an optimum geometrical configuration for practical design [4, 5, 6, 7, 8].

Until now, on the vertical-axis Savonius wind turbine both aerodynamic and structural works have been done in many parts of the world. Huda et al. [9] investigated the aerodynamic forces acting on a stationary S-shaped rotor and made an attempt to predict the dynamic performances from these forces. Islam et al. [10] analyzed the performance of S-shaped rotor by placing a flat plate in

front of the returning blade. Gavalda et al. [11] analyzed the drag and lift coefficient of Savonius wind machine, in order to obtain quantitative information about the aerodynamic performance of the Savonius rotor. However, little attention has been given on the static and dynamic characteristics when the number of blade of the savonius rotor is increased.

The present research work is consisted of finding static drag coefficients at the normal and tangential direction of the chord, static torque coefficient for individual blade C_q, total static torque coefficient C_Q at a fixed Reynolds number of a six bladed savonius rotor at different angle of rotation ranging from $\alpha = 0^o$ to 360^o by measuring the surface pressures of blades. The quasi-steady approach applied to the analysis of a Darrieus rotor has been finally considered for predicting the performance of the six bladed Savonius rotor.

2 SIX BLADED SAVONIUS ROTOR

The Savonius rotor was made up of three half cylinders (blade) of diameter, d=101 mm and height H=300mm. The cylinders were made of PVC material. The overlap distance S was selected to be one third of the cylinder diameter (i.e., S=a/d=0.3) and the central shaft had been removed. The overlap distance selected was the optimum value with respect to the wind power extraction. The whole rotor was fixed on an iron frame by using two side shafts and two ball bearings. The pressure measurements were made at 13 pressure tapping points on each two blades which are shown in **Fig.1**.

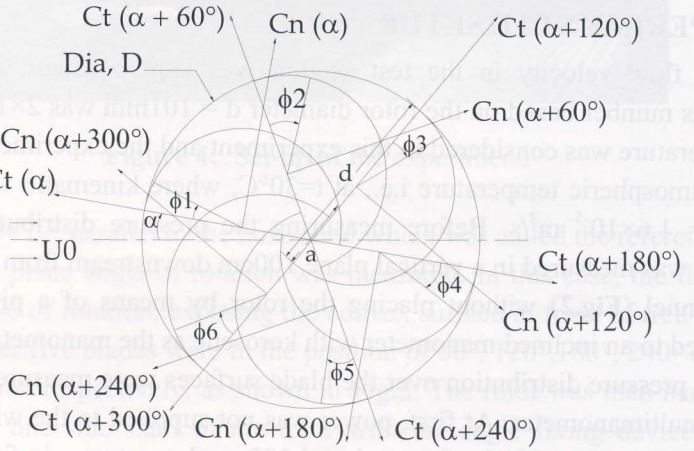

Figure 1: Forces acting on blades.

1. **Converging mouth entry**
2. **Perspex section**
3. **Rectangular diverging section**
4. **Fan section**
5. **Butterfly section**
6. **Silencer with honeycomb section**
7. **Diverging section**
8. **Converging section**
9. **Rectangular section**
10. **Flow straightner section**
11. **Rectangular exit section**

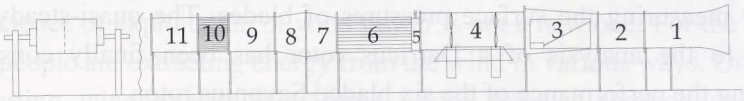

Figure 2: Schematic diagram of wind tunnel.

The tappings were made with copper tubes of 1.5mm outer diameter and 10mm length which were press fitted to the tapping holes. The tappings were located at the mid-plane of one side of each blade, so that pressure distribution at every 10° on the blade surface could be measured. The pressure tappings were connected to a inclined multimanometer (manometric fluid was water and had an accuracy of ± 0.1 mm of water column) through 2mm PVC tubes. The pressures were measured at every 10° interval of rotor angle so that a detailed picture of the aerodynamic loading and torque characteristics could be obtained.

3 EXPERIMENTAL SETUP

The flow velocity in the test section was kept constant at 13m/s. The Reynolds number based on the rotor diameter d = 101mm was 2×10^5. The effect of temperature was considered in this experiment and the experiment was carried out at atmospheric temperature i.e., at t=30°C, where kinematic viscosity of air was $\nu = 1.6\times10^{-5}$ m^2/s. Before measuring the pressure distribution the mean velocity was measured in a vertical plane 100cm downstream from the exit of the wind tunnel (**Fig.2**) without placing the rotor by means of a pitot static tube connected to an inclined manometer with kerosene as the manometric fluid.

The pressure distribution over the blade surfaces were measured step by step by the multimanometer. At first, power was not supplied to the wind tunnel and the Savonius rotor with the frame placed 100cm downstream in front of the exit section of the tunnel on a table. Fix one blade of the rotor parallel to the free

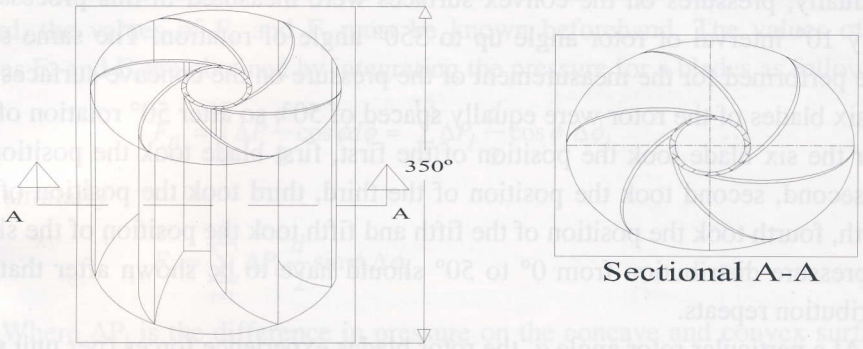

Figure 3: Cross-sectional and three dimensional view of six bladed Savonius rotor.

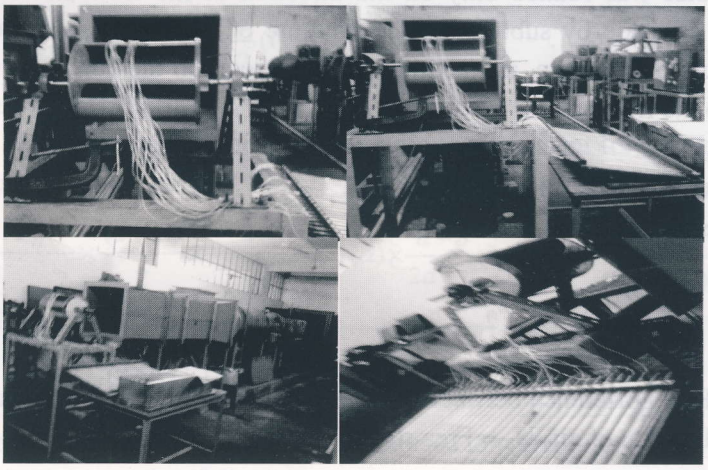

Figure 4: Set-up of the experiment.

stream velocity i.e. parallel to the horizontal which was called the reference plane and from this plane angle of rotation was measured. In this case, the first blade was at 0° angle of rotation, exposing the convex surface in front of free steam of air, so the other five blades were in the position of 60°, 120°,180°, 240° and 300° angle of rotation respectively, as shown in **Fig.3**. The rotor was then made static by fixing the one side shaft of the rotor with the angle fixing device (**Fig.4**). Power of the tunnel then made on to flow the free stream of air with uniform velocity over the blades of the rotor. Pressure on the convex surface of blades was measured at a particular rotor angle α, fixing the rotor at static condition.

Gradually, pressures on the convex surfaces were measured in this process for every 10° interval of rotor angle up to 350° angle of rotation. The same steps were performed for the measurement of the pressure on the concave surfaces. As the six blades of the rotor were equally spaced of 50°, so after 50° rotation of the rotor the six blade took the position of the first, first blade took the position of the second, second took the position of the third, third took the position of the fourth, fourth took the position of the fifth and fifth took the position of the sixth. So pressure distribution from 0° to 50° should have to be shown after that the distribution repeats.

At a particular rotor angle α, the rotor blades experience forces (per unit span length) due to the pressure difference between the concave surface and the convex surface and these forces can be resolved into two components F_n and F_t. Since the blade surfaces are circular, F_n and F_t are shown in **Fig.1**. It was noted that, the rotor was rotated only on the direction of the flow and the pressure difference as made by subtracting the pressure of the convex surface from the concave surface pressure, as maximum time of rotation the concave surface was exposed to the free stream.

3.1 Pressure Co-efficient, C_P

Pressure coefficient is defined as

$$C_p = \frac{P - P_o}{\frac{1}{2}\rho U_o^2} \quad \ldots \quad \ldots \quad \ldots \quad \ldots \quad (1)$$

Where, $P-P_o$ = Difference between bade and atmospheric pressure in pascal and
ρ = Density of air, U_o = Free stream velocity

3.2 Drag Coefficient

The drag coefficient in normal and tangential directions can be written as follows:

$$C_n = \frac{F_n}{\frac{1}{2}\rho U_o^2 d} \quad \ldots \quad \ldots \quad \ldots \quad \ldots \quad (2)$$

$$C_t = \frac{F_t}{\frac{1}{2}\rho U_o^2 d} \quad \ldots \quad \ldots \quad \ldots \quad \ldots \quad (3)$$

To obtain the drag coefficients in the normal and tangential direction of the chord, the values of F_n and F_t must be known beforehand. The values of the forces F_n and F_t are obtained by integrating the pressure for a blades as follows:

$$F_n = \int_0^{\pi} \Delta P \frac{d}{2} \cos\phi d\phi = \sum_{i=1}^{13} \Delta P_i \frac{d}{2} \cos\phi_i \Delta\phi_i \quad \ldots \quad (4)$$

and similarly

$$F_t = \sum_{i=1}^{\pi} \Delta P_i \frac{d}{2} \sin\phi_i \Delta\phi_i \quad \ldots \quad \ldots \quad \ldots \quad (5)$$

Where ΔP_i is the difference in pressure on the concave and convex surfaces at particular pressure tapping, i. Where F_n is responsible for producing a torque on the shaft of the rotor and this torque can be expressed for a blade as

Torque on a blade,

$$T = F_n \times \frac{d-a}{2} = F_n \times \frac{d}{2}(1-\frac{a}{d}) = F_n \times \frac{d}{2}(1-s) \quad \ldots \quad \ldots \quad (6)$$

3.3 Torque Coefficient

Equation (4) can be reduced to get the torque coefficient for a single blade at a particular rotor angle as

$$C_q(\alpha) = \frac{F_n}{\frac{1}{2}\rho U_0^2} \times \frac{(d-a)}{2} \times \frac{2}{2d-a} = C_n(\alpha) \times \frac{d-a}{2d-a} = C_n(\alpha) \times \frac{d(1-a/d)}{d(2-a/d)}$$

$$C_q(\alpha) = C_n(\alpha)\frac{(1-s)}{(2-s)} \quad \ldots \quad \ldots \quad \ldots \quad (7)$$

The total static torque coefficient produced on the rotor shaft by the six blades can be expressed as follows:

$$C_Q = \frac{(F_1+F_2+F_3+F_4+F_5+F_6)}{\frac{1}{2}\rho U_o^2} \times \frac{\frac{(d-a)}{2}}{\frac{(2d-a)}{2}} = \frac{(F_1+F_2+F_3+F_4+F_5+F_6)}{\frac{1}{2}\rho U_o^2} \times \frac{d-a}{2d-a} \times \frac{d}{D}$$

$$C_Q = \begin{bmatrix} C_n(\alpha)+C_n(\alpha+60°) \\ +C_n(\alpha+120°)+C_n(\alpha+180°) \\ +C_n(\alpha+240°)+C_n(\alpha+300°) \end{bmatrix} \times \frac{(1-s)}{(2-s)^2} \quad \ldots \quad \ldots \quad (8)$$

Where $C_n(\alpha)$, $C_n(\alpha+60°)$, $C_n(\alpha+120°)$, $C_n(\alpha+180°)$, $C_n(\alpha+240°)$, and $C_n(\alpha+300°)$ refer to the drag coefficients of the first, second, third, four, five and six blade respectively at rotor angle α.

3.4 Power Coefficient

$$C_n' = C_n(\alpha)\times(V_{w1}/U_o)^2 \quad \ldots \quad \ldots \quad (9)$$

$$C_n'(60+\alpha) = C_n(60+\alpha)\times(V_{w2}/U_o)^2 \quad \ldots \quad \ldots \quad (10)$$

$$C_n'(120+\alpha) = C_n(120+\alpha)\times(V_{w3}/U_o)^2 \quad \ldots \quad \ldots \quad (11)$$

$$C_n'(180+\alpha) = C_n(180+\alpha)\times(V_{w4}/U_o)^2 \quad \ldots \quad \ldots \quad (12)$$

$$C_n'(240+\alpha) = C_n(240+\alpha)\times(V_{w5}/U_o)^2 \quad \ldots \quad \ldots \quad (13)$$

$$C_n'(300+\alpha) = C_n(300+\alpha)\times(V_{w6}/U_o)^2 \quad \ldots \quad \ldots \quad (14)$$

Power coefficient at α,

$$C_p(\alpha) = C_Q(\alpha).\lambda \quad \ldots \quad \ldots \quad \ldots \quad (15)$$

A computer programme was performed to calculate the power coefficient (C_P) using the value of the component of relative velocity V_W along U_o and static normal drag coefficient $C_n(\alpha)$ for three different tip speed ratio λ with the help of equations (7) to (12).The program output gave three sets of dynamic torque coefficients and power coefficient and finally three average value of power coefficient C_{Pave}.

Power coefficient vs. tip speed ratio of the present prediction and the previous researchers' prediction were plotted on the same graph for analysis.

4 RESULTS AND DISCUSSION

The results of experimental investigation conducted for the wind tunnel flow over the six bladed Savonius rotor. The results of the pressure distribution over the convex and concave surfaces of each blade at different angle of rotation are analyzed first. Nature of the drug and static torque characteristics are also analysed. This topic includes the analysis of pressure distribution, normal drag coefficient (C_n), tangential drag coefficient (C_t), torque coefficient (C_q), and total static torque coefficient (C_Q).

4.1 Pressure Distribution

The pressure distributions over the surfaces of the blades were measured at every 10° interval of the rotor angle between $0° \leq \alpha \leq 50°$. The results are presented in the (**Fig. 5-10**).

At rotor angle α=0° (**Fig. 5**) as the flow accelerates over the leading edge of the convex surface of the first blade, the pressure decreases up to φ_1=67.5°. The flow separation occurs at φ_1=67.5° by an adverse pressure gradient on the first blade of the convex surface and becomes negative value. After that pressure

smoothly increases from pressure tapping angle φ_1= 67.5° to φ_1= 180°.The pressure increases to positive value from φ_2 = 0° to φ_2 =22.5° for the second blade and then decreases from φ_2 =22.5° to φ_2 =67.5° to negative value. From φ_2 =67.5° to φ_2 =180°, pressure again increases. On the third blade, pressure decreases in the negative values between φ_3 =22.5° to φ_3 =45° and then pressure remains constant. Whereas, on the fourth blade pressure decreases from φ_4 =22.5° to φ_4 =45° and after that it remains almost constant. However, on the fifth blade pressure increases from φ_5 =0° to φ_5 =45° and then decreases from φ_5 =40° to φ_5 =90° and then again it increases from φ_5 =90°. On the sixth blade pressure increases from φ_6 =0° to φ_6 =22.5° and decreases from φ_6 =22.5° to φ_6 =45° and after φ_6 =45° it started increasing to positive value.

Considering the concave surface of the first blade pressure remains approximately constant. On the second blade, pressure fluctuates slightly in positive values from φ_2 =0° to φ_2 =67.5°. From the pressure tapping angle φ_2 =67.5° to φ_2 =180°, pressure slightly increases. In the case of the third blade pressure remains constant from φ_3 =0° to φ_3 =90° and then decreases up to φ_3 =135°. From φ_3 =135° to φ_3 =180°, it slightly increases. However, on the fourth, fifth and sixth blades pressure remains almost constant value from φ =0° to φ =180°.

At rotor angle α=10° (**Fig. 6**) pressure on the convex surface of the first blade decreases up to φ_1 =67.5°. The flow separation occurs at φ_1 =67.5° by an adverse pressure gradient on the first blade on the convex surface and becomes negative. The pressure increases after φ_1 =67.5° to φ_1 =180°. On the second blade pressure increases to positive value from φ_2 =0° to φ_2 =22.5° and then decreases from φ_2 =22.5° to φ_2 =67.5° to negative value. From the pressure tapping angle φ_2 =67.5° to φ_2 =90°, pressure again increases. Again, pressure decreases from φ_2 =90° to φ_2 =112.5° and then increases from φ_2 =112.5° to φ_2 =180°. Whereas, on the third blade pressure increases from φ_3 =0° to φ_3 =22.5° and then pressure decreases to negative value from φ_3 =22.5° to φ_3 =67.5°. Again, pressure increases from φ_3 =67.5° to φ_3 =135° and after φ_3 =135° to the pressure tapping angle φ_3=180° pressure remains constant. On the fourth blade, pressure remains almost constant. In the case of the fifth blade, pressure increases from φ_5 =0° to φ_5 =180° smoothly. The pressure increases from φ_6 =0° to φ_6 =112.5° on the sixth blade and then decreases from φ_6 =112.5° to φ_6 =180° and reaches to negative value.

The pressure remains approximately constant on the concave surface of the first blade. On the second blades pressure fluctuates slightly in positive values

from φ_2 =0° to φ_2 =67.5°. Again from pressure tapping angle φ_2=67.5° to φ_2 =180°, pressure remains constant. On the third blade, pressure coefficient C_{px} fluctuates slightly. It is found that on the fourth, fifth and sixth blade, pressure distribution over the concave surfaces shows the same characteristics as for α=0°.

From the (**Fig. 7**) at rotor angle α=20°, it is found that the pressure on the convex surface of the first blade decreases from φ_1=0° to φ_1=67.5°. The flow separation occurs at φ_1=67.5° by an adverse pressure gradient on the first blade of the convex surface and becomes negative value. The pressure increases from φ_1=67.5° to φ_1=180°. For the second blade, pressure increases to positive value from φ_2 =0° to φ_2 =22.5° and then decreases from φ_2 =22.5° to φ_2 =67.5° to negative value and pressure again increases from φ_2=67.5° to φ_2=180°. Whereas, on the third blade pressure decreases from φ_3=0° to φ_3=67.5° and then again pressure increases from φ_3=67.5° to φ_3=180°. However, on the fourth blade pressure remains almost constant. But on the fifth blade pressure increases from φ_5=0° to φ_5=67.5° smoothly. Then from pressure tapping angle φ_5=67.5° to φ_5=90° pressure decreases and again increases from φ_5=90° to φ_5=180°. For the sixth blade pressure increases from φ_6=0° to φ_6=112.5° and decreases in the range of pressure tapping angle φ_6=112.5° to φ_6=180° and reaches to the negative value.

It is found that on the concave surface of the first blade pressure fluctuates slightly. However, on the second blade pressure remains almost constant at atmospheric level. For the third blade, the pressure coefficient C_{px} decreases from φ_3=0° to φ_3=67.5° and increases in the range of φ_3=67.5° to φ_3=135° and then remains almost constant. Whereas, on the fourth, fifth and sixth blade, pressure distribution over the concave surface shows the same characteristics at rotor angle of α=10°.

When the rotor angle α=30° (**Fig. 8**), the pressure on the convex surface of the first blade decreases from φ_1=0° to φ_1=67.5°. The flow separation occurs at φ_1=67.5° by an adverse pressure gradient on the first blade of the convex surface and becomes negative value. Pressure increases from φ_1=67.5° to φ_1=180°. On the second blade, pressure distribution over the convex surface shows the same characteristics as for α=20°. It is found that pressure decreases from φ_3=0° to φ_3=67.5° on the third blade. Then pressure increases in the negative value from φ_3=67.5° to φ_3=135° and remains constant. On the fourth blade, pressure decreases from φ_4=0° to φ_4=67.5° and increases from φ_4=67.5° to φ_4=135° and then remains almost constant. Whereas, on the fifth blade pressure increases from φ_5=0° to φ_5=67.5° smoothly. It decreases from φ_5=67.5° to φ_5=90° and

again increases from φ_5=90° to,φ_5=180°. On the sixth blade, pressure distribution over the convex surfaces shows the same characteristics as for α=20° with slightly different in the separation point.

In case of the concave surface of the first blade pressure fluctuates slightly. On the second blade pressure remains constant at atmospheric level. On the third blade, the C_{px} decreases from φ_3=0° to φ_3=67.5°. It increases from φ_3=67.5° to φ_3=135° and then remains constant. The pressure distribution on the fourth and fifth blade over the concave surfaces shows the same characteristics as for α=20°. However, on the sixth blade pressure slightly decreases in negative value from φ=0° to φ=180°.

Considering the rotor angle α=40° (**Fig. 9**), the pressure on the convex surface of the first blade decreases up to φ_1=67.5° and then increase from φ_1=67.5° to φ_1=180°. On the second blade, pressure decreases from φ_2=0° to φ_2=67.5° and then increases from φ_2=67.5° to φ_2=180°. On the third blade, pressure decreases from φ_3=67.5° to φ_3=90° and increases from φ_3=90° to φ_3=180°. But on the fourth blade, pressure fluctuates slightly between φ_4=0° to φ_4=180°. Whereas, on the fifth blade, pressure increases from φ_5=0° to φ_5=135° smoothly and decreases from φ_5=135° to φ_5=180°. For the sixth blade, pressure at first increases from φ_6=0° to φ_6=22.5° and then decreases from φ_6=22.5° to φ_6=67.5°. Again, pressure increases from φ_6=67.5° to φ_6=135° pressure tapping angle and again started decreasing from φ_6=135°.

For the concave surface of the first blade pressure fluctuates slightly. But on the second blade pressure remains constant at atmospheric level. However, on the third blade, pressure distribution over the concave surfaces shows the same characteristics as for α=30°. On the fourth blade, pressure distribution over the concave surfaces shows the same characteristics as for α=20°. On the fifth blade, pressure coefficient C_{pe} remains almost constant from φ=0° to φ=180°.

When the rotor angle α=50° (**Fig. 10**) pressure on the convex surface of the first blade decreases from φ_1=0° to φ_1=67.5°. The flow separation occurs at φ_1=67.5° by an adverse pressure gradient on the first blade of the convex surface and then increases from φ_1=67.5° to φ_1=180°. On the second blade pressure decreases from φ_2=0° to φ_2=67.5° and increases from φ_2=67.5° to φ_2=135° and then it again decreases. But on the third blade, pressure distribution over the convex surface shows the same characteristics as for α=40°. On the fourth blade pressure fluctuates between φ_4=0° to φ_4=180°. Whereas, on the fifth blade pressure increases from φ_5=0° to φ_5=135° smoothly and decreases from φ_5=135°

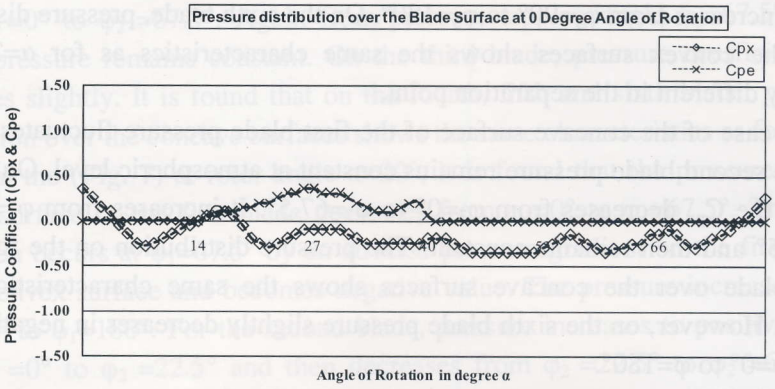

Figure 5: Pressure distribution over the blade surfaces at 0° angle of rotation.

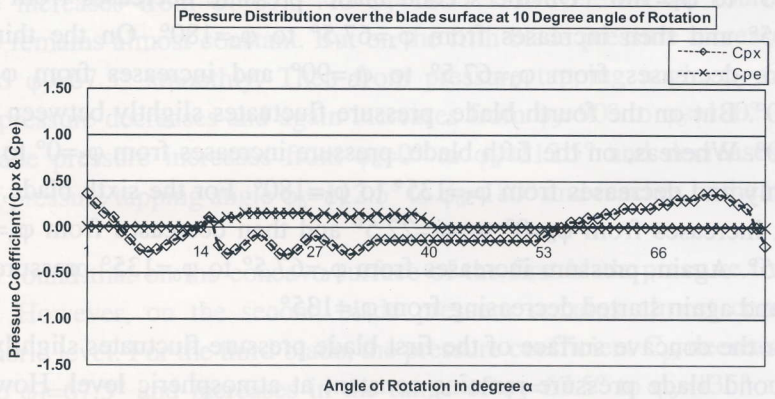

Figure 6: Pressure distribution over the blade surfaces at 10° angle of rotation.

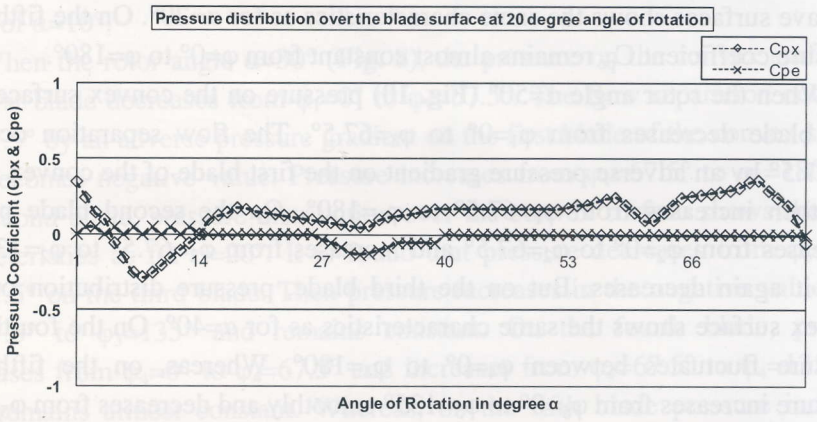

Figure 7: Pressure distribution over the blade surfaces at 20° angle of rotation.

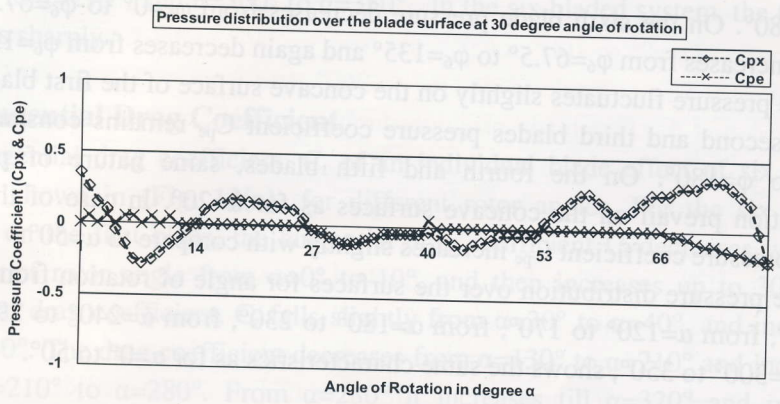

Figure 8: Pressure distribution over the blade surfaces at 30° angle of rotation.

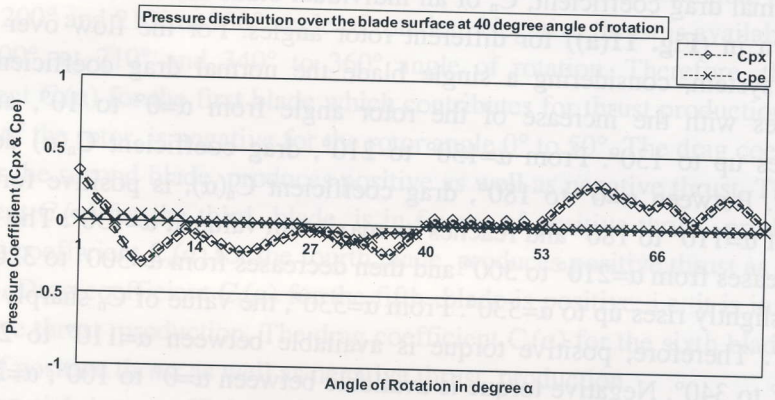

Figure 9: Pressure distribution over the blade surfaces at 40° angle of rotation.

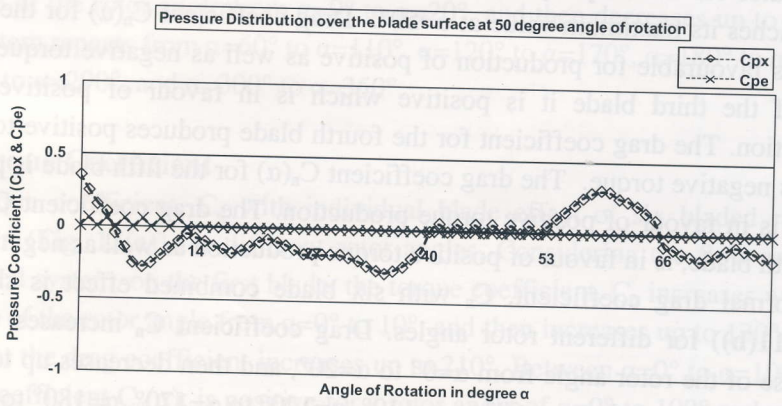

Figure 10: Pressure distribution over the blade surfaces at 50° angle of rotation.

to φ_5=180°. On the sixth blade pressure decreases from φ_6=0° to φ_6=67.5° and then it increases from φ_6=67.5° to φ_6=135° and again decreases from φ_6=135°.

The pressure fluctuates slightly on the concave surface of the first blade. But on the second and third blades pressure coefficient C_{pe} remains constant from φ=0° to φ=180°. On the fourth and fifth blades, same nature of pressure distribution prevail on the concave surfaces as for α=20°. In case of the sixth blade, pressure coefficient C_{pe} increases slightly with compare to α=50°.

The pressure distribution over the surfaces for angle of rotation from α=60° to 110°, from α=120° to 170°, from α=180° to 230°, from α=240° to 290°, and from α=300° to 350°, shows the same characteristics as for α=0° to 50°.

4.2 Normal Drag Coefficient

Normal drag coefficient, C_n of an individual blade effect of six bladed rotor is shown in (**Fig. 11(a)**) for different rotor angles. For the flow over the six bladed system, considering a single blade the normal drag coefficient $C_n(\alpha)$ decreases with the increase of the rotor angle from α=0° to 10°, and then increases up to 130°. From α=130° to 210°, drag coefficient $C_n(\alpha)$ decreases linearly. Between α=0° to 180°, drag coefficient $C_n(\alpha)$, is positive for a rotor angle of α=110° to 180° and reaches its maximum value at α=130°. The value of C_n increases from α=210° to 300° and then decreases from α=300° to 320°. After that it slightly rises up to α=330°. From α=330°, the value of C_n sharply falls till α=360°. Therefore, positive torque is available between α=110° to 200° and α=220° to 340°. Negative torque is available between α=0° to 100°, α=210° and α=350° to α=360°. Therefore, the drag coefficient $C_n(\alpha)$ for the first blade contributes for the torque production, is negative for a rotor angle of 0° to 50° and reaches its maximum value at α=50°. Drag coefficient $C_n(\alpha)$ for the second blade is favourable for production of positive as well as negative torque. In the case of the third blade it is positive which is in favour of positive torque production. The drag coefficient for the fourth blade produces positive torque as well as negative torque. The drag coefficient $C_n(\alpha)$ for the fifth blade is positive, which is in favour of positive torque production. The drag coefficient $C_n(\alpha)$ for the sixth blade, is in favour of positive torque production as well as negative.

Normal drag coefficient, C_n with six blade combined effect is shown in (**Fig. 11(b)**) for different rotor angles. Drag coefficient C_n increases with the increase of the rotor angle from α=0° to α=20°, and then decreases up to α=60°. The system repeats from α=60° to α=110°, α=120° to α=170°, α=180° to α=230°,

α=240° to α=290°, and α=300° to α=350°. In the six bladed system, the C_n rises and falls sharply.

4.3 Tangential Drag Coefficient

Tangential drag coefficient, C_t of an individual blade effect of six bladed rotor is shown in (**Fig. 12(a)**) for different rotor angles. For the six bladed system, on the first blade, the tangential drag coefficient C_t decreases with the increase of rotor angle from α=0° to 10°, and then increases up to 30°. The tangential drag coefficient, C_t falls slightly from α=30° to α=40°, and increases up to 130°. The drag coefficient decreases from α=130° to α=210° and increases from α=210° to α=280°. From α=280° it increases till α=320° and remains constant at to α=330°. The drag coefficient, C_t decreases sharply from α=330° to α=350° and then remains constant to α=360°. Positive thrust is available between 110° to 200° and 210° to 330° angle of rotation. Negative thrust is available from 0° to 100°, at 210° and 340° to 360° angle of rotation. Therefore, the drag coefficient $C_t(\alpha)$ for the first blade which contributes for thrust production in the support of the rotor, is negative for the rotor angle 0° to 50°. The drag coefficient $C_t(\alpha)$ for the second blade, produces positive as well as negative thrust. The drag coefficient $C_t(\alpha)$ for the third blade, is in favour of positive thrust production. The drag coefficient $C_t(\alpha)$ for the fourth blade, produces positive thrust as well as negative. Drag coefficient $C_t(\alpha)$ for the fifth blade is positive, i.e. it is in favour of positive thrust production. The drag coefficient $C_t(\alpha)$ for the sixth blade, is in favour of positive thrust as well as negative thrust production.

Tangential drag coefficient, C_t with six blades combined effect is shown in (**Fig. 12(b)**) for different rotor angles. Drag coefficient C_t increases with the increase of the rotor angle from α=0° to α=20°, and then decreases up to α=60°. The system repeats from α=60° to α=110°, α=120° to α=170°, α=180° to α=230°, α=240° to α=290°, and α=300° to α=350°.

4.4 Torque Coefficient

Torque coefficient, C_q with individual blade effect of six bladed rotor is shown in (**Fig. 13(a)**) for different rotor angles. Considering the flow over the six-bladed system, on the first blade, the torque coefficient, C_q increases with the increase of the rotor angle from α=0° to 10°, and then increases up to 130°. From this point the drag coefficient increases up to 210°. Between α=0° to α=100°, the torque coefficient $C_q(\alpha)$, is positive for a rotor angle of α=0° to 100° and reaches its maximum value at α=10°. The coefficient decreases from α=210° to 300°. It

increases from α=330° to α=360°. Therefore, the positive torque is available for a rotor angle of α=0° to 100° at 210° and from α=340° to 360°. Negative torque is available for a rotor angle of α=110° to 200°, and from α=220° to α=330°. It is observed that the first blade produces highest torque among the six blades. For the six-bladed system, the nature of this curve is opposite to that of the normal drag coefficient, C_n with the individual blade effect, which is responsible for producing torque. The different is that the value of torque coefficient is smaller than normal drag coefficient with individual blade effect.

Total static torque coefficient, C_q with six blades vane rotor is shown in (**Fig. 13(b)**) at different rotor angles. For the six-bladed system, the nature of the curve repeats after 50° angle of rotation like that of the normal drag coefficient due to combined effect. The value of torque coefficient is smaller than that of normal drag coefficient with combined blade effect. And total static torque coefficient is positive where normal drag coefficient for combined blade effect is negative value. Here the total static torque decreases with the increase of the rotor angle up to α=20°. From this point the coefficient C_q increases till α=60°. Then the curve repeats. The curve repeats from α=60° to α=110°, α=120° to α=170°, α=180° to α=230°, α=240° to α=290°, and α=300° to α=350°.

4.5 Power Coefficient

The predicted power coefficients for different tip speed ratios are shown in (**Fig. 14**) along with the measured data of Ogawa & Yashida [8] and Islam et. al. [12]. The rotor of Ogawa & Yashida, Islam et al have the same overlap ratio of the one considered in this study. The predicted power coefficient matches qualitatively with the measured data, but shows a great deviation. The power coefficient values have been found in between 0.02 to 0.157.

Accordingly, it has been observed from the comparisons graph shown in (**Fig.15**) that the value of power coefficient (C_P) with the six bladed effects in this study coincides with the values of power coefficient in the literature studies. As seen in figure, the maximum power coefficient has been obtained around 0.9 value of tip speed ratio (λ) for all arrangements. The present prediction method assumes a potential vortex, however, in reality the flow field around a rotating rotor is governed by time dependent shear layers, separated flows and high turbulence levels. Furthermore, the wake has not been considered in the present study.

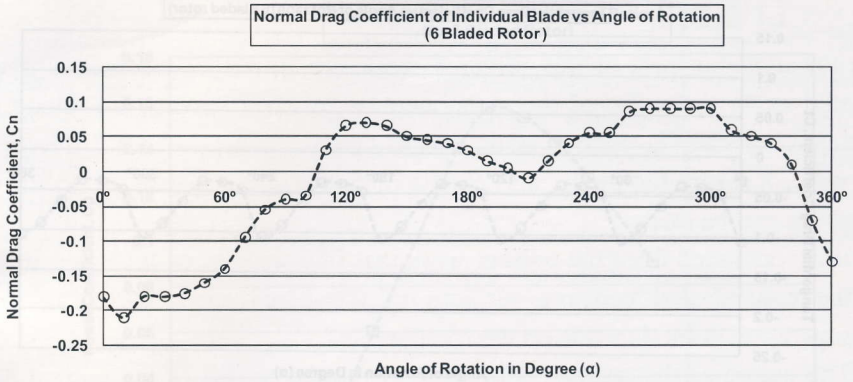

Figure 11(a): Normal Drag Coefficient with Individual blade effect (6 bladed rotor).

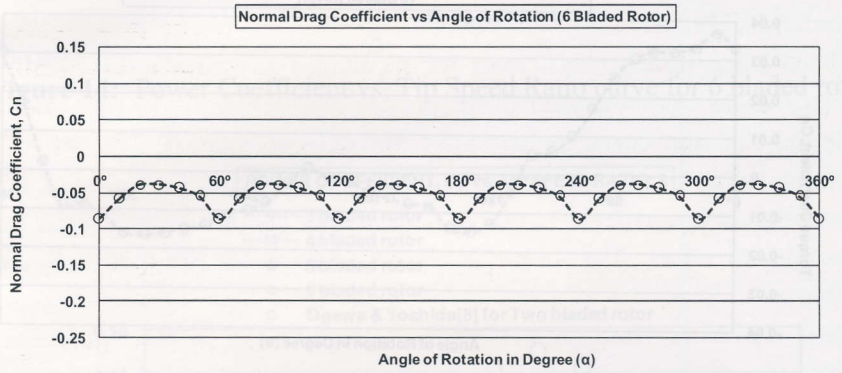

Figure 11(b): Normal Drag Coefficient with Combined blade effect (6 bladed rotor)

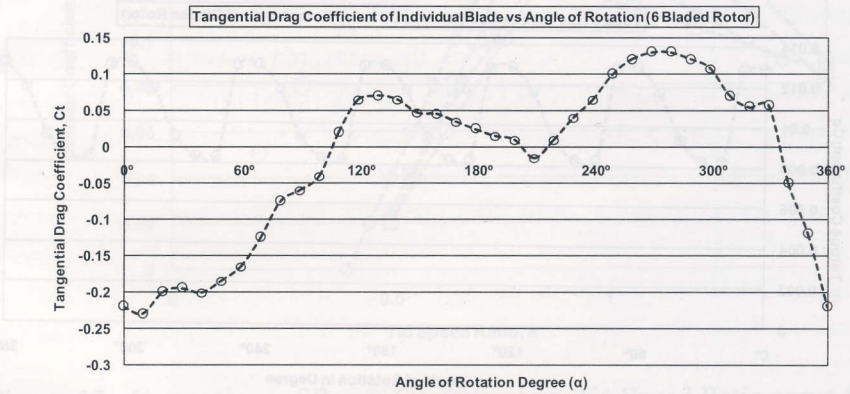

Figure 12(a): Tangential Drag Coefficient with Individual blade effect (6 bladed rotor)

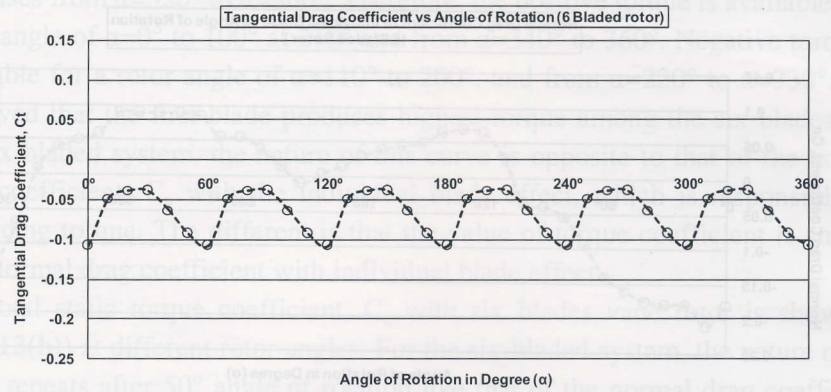

Figure 12(b): Tangential Drag Coefficient with Combined blade effect (6 bladed rotor)

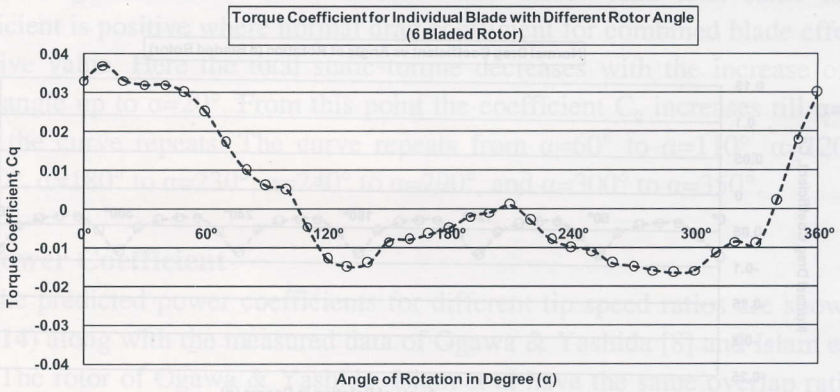

Figure 13(a): Torque Coefficient with Individual blade effect (6 bladed rotor).

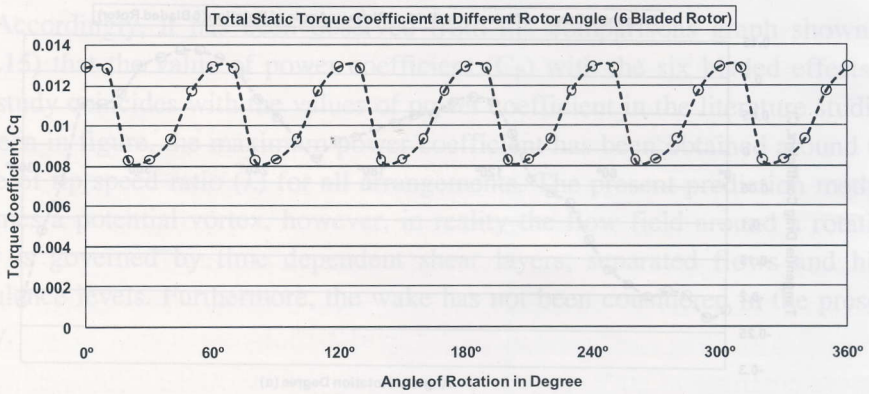

Figure 13(b): Torque Coefficient with Combined blade effect (6 bladed rotor).

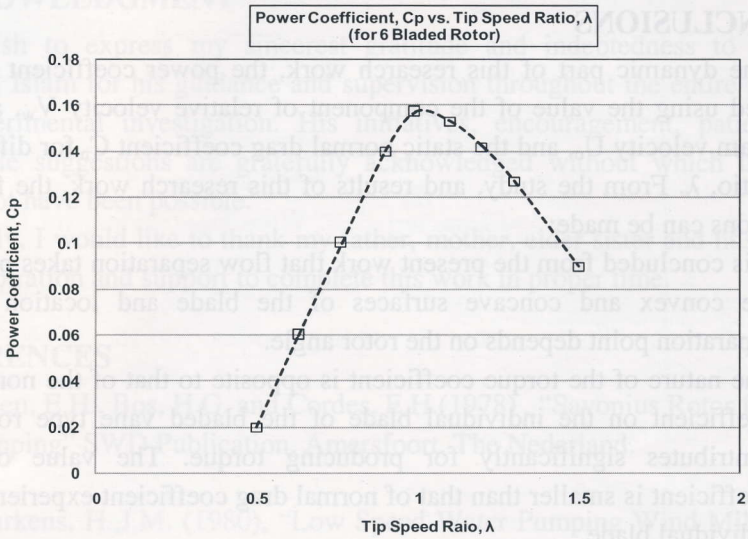

Figure 14: Power Coefficient vs. Tip Speed Ratio curve for 6 bladed rotor.

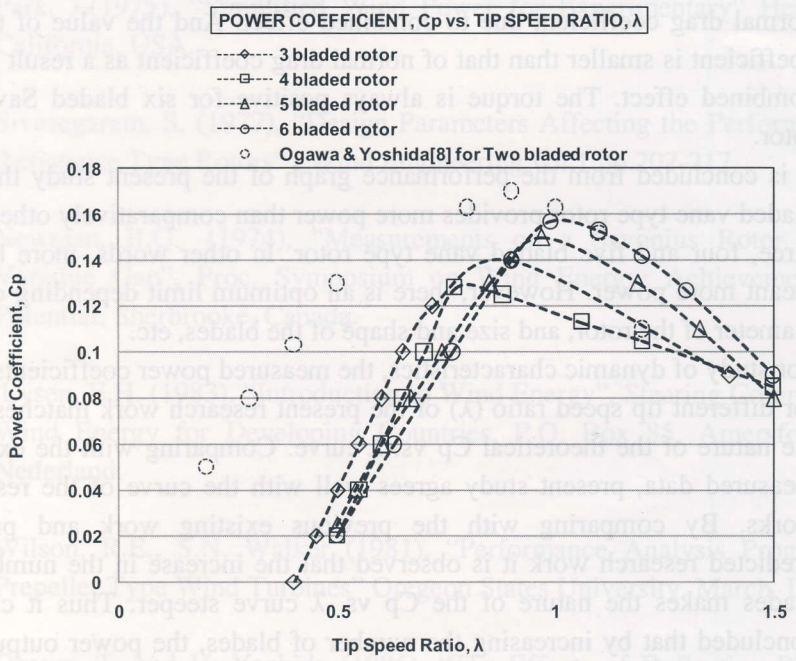

Figure 15: Comparison of Power Coefficient vs. Tip Speed Ratio curve for different type of rotor.

5 CONCLUSIONS

In the dynamic part of this research work, the power coefficient (C_p) was calculated using the value of the component of relative velocity V_w, along the free stream velocity U_o, and the static normal drag coefficient C_n for different tip speed ratio, λ. From the study, and results of this research work, the following conclusions can be made:

(i) It is concluded from the present work that flow separation takes place over the convex and concave surfaces of the blade and location of such separation point depends on the rotor angle.

(ii) The nature of the torque coefficient is opposite to that of the normal drag coefficient on the individual blade of the bladed vane type rotor. This contributes significantly for producing torque. The value of torque coefficient is smaller than that of normal drag coefficient experienced with individual blade.

(iii) Total static torque coefficients for six bladed Savonius rotor at different rotor angle were analyzed in the present research work. In this case, it is found that the curve repeats after 50°angle of rotation like that of the normal drag coefficient due to combined effect. And the value of torque coefficient is smaller than that of normal drag coefficient as a result of the combined effect. The torque is always positive for six bladed Savonius rotor.

(iv) It is concluded from the performance graph of the present study that six bladed vane type rotor provides more power than comparatively other two, three, four and five bladed vane type rotor. In other words, more blades meant more power. However, there is an optimum limit depending on the diameter of the rotor, and size and shape of the blades, etc.

(v) For study of dynamic characteristics, the measured power coefficients (Cp) for different tip speed ratio (λ) of the present research work matches with the nature of the theoretical Cp vs. λ curve. Comparing with the existing measured data, present study agrees well with the curve of the research works. By comparing with the previous existing work and present predicted research work it is observed that the increase in the number of blades makes the nature of the Cp vs. λ curve steeper. Thus it can be concluded that by increasing the number of blades, the power output can also be increased.

ACKNOWLEDGMENT

I wish to express my sincerest gratitude and indebtedness to Dr. Md. Quamrul Islam for his guidance and supervision throughout the entire period of the experimental investigation. His initiatives, encouragement, patience and invaluable suggestions are gratefully acknowledged without which this work would not have been possible.

Lastly, I would like to thank my father, mother, elder sister and husband for their inspiration and support to complete this work in proper time.

REFERENCES

[1] Lysen, E.H., Bos, H.G. and Cordes, E.H.(1978) , "Savonius Rotor for Water Pumping" SWD Publication, Amersfoort, The Nederland.

[2] Beurkens, H.,J.M. (1980), "Low Speed Water Pumping Wind Mills: Rotor Tests and overall performance", Proc. Of 3ed Int. Symp. On Wind Energy System, Copenhagen, Denmark.

[3] Park, J.(1975), "Simplified Wind Power for Experimentary" Helion In., California, USA.

[4] Sivasegaram, S. (1977), "Design Parameters Affecting the Performance of Resistance Type Rotors" , Wind Engineering vol.1,pp.207-217.

[5] Newman, B.G.. (1974), "Measurements on a Savonius Rotor With a Variable Gap", Proc. Symposium on Wind Energy: Achievements and Potential, Sherbrooke, Canada.

[6] Lysen, E.H. (1983), "Introduction to Wind Energy", Steering Committee of Wind Energy for Developing Countries, P.O. Box 85, Amersfoort, the Nederland.

[7] Wilson, R.E., S.N. Walker (1981), "Performance Analysis Program for Prepeller Type Wind Turbines" Oregeon States University, March, USA.

[8] Ogawa, T. and H. Yoshida (1986), "The Effects of Deflecting Plate and Rotor Plate" Bull. JSME, vol. 29, pp. 2115-2121.

[9] Huda, M.D., Selim, M.A., Islam A.K.M.S and Islam, M.Q. (1992) "The Performance of an S-shaped Savonius Rotor with a Deflecting Plate", RERIC Int. Energy Journal, Vol. 14, No. 1, pp. 25-32.

[10] Islam, A.K.M.S., Islam, M.Q., Razzaque, M.M. and Ashraf, R. (1995), "Static Torque and Drag Characteristics of an S-Shaped Savonius Rotor and Prediction of Dynamic Characteristics", Wind Engineering, vol.19, no. 6.

[11] Gavalda, J., Massons, J. and Diaz, F. (1991), "Drag and lift coefficients of the Savonius Wind machine", Wind Engineering, vol. 15, pp. 240-246.

(Contd. from 2nd cover page)

8. SI units must be used in the manuscript. However, other units may be used in parenthesis.

9. Tables should be referred to in consecutive Arabic numerical. Each table must have a table caption.

10. Line drawings must be in a form suitable for reproduction e.g., laser printout, drawn in Indian ink on white paper or on tracing paper. Photographs should have a glossy finish. Each figure must have a number and a figure caption. Elecrtonic mode is preferred.

11. References should be set out in alphabetical order of the author's last name in a list at the end of the article. They should be given in standard form as in the following examples :

(a) Journal

Bloomer G and Wright A. (1984) Scheduling of Vehicles from Factory to Depot. *Journal of Vehicles*, Vol. 12: pp. 590-598.

(b) Book

Best, John., and Kahn, James V., Research in Education, Prentice-Hall, New Jersey, 1986.

(c) Monograph

Syedali, M.M. "Computer Controlled Car", Thesis, M.Sc. Engineering, Department of Mechanical Engineering, BUET, 1990

(d) Conference Paper

Hasan M and Ullah MS. "Tourism development in the Chittagong Hill Tracts of Bangladesh after the peace agreement of 1997", a paper submitted to the Regional Conference on physical mobility and development in the mountains", Tribhuvan University, 15-17, March, 2000 Kathmandu, Nepal, pp.12

(e) Unpublished paper

Ahmadi, R and Tangs : Production Allocation with Dual Provisioning, Working Paper, Anderson Graduate School of Management, UCLA (1991)

12. The University does not accept responsibility for loss or damage of manuscript while in mail.

13. The responsibility for opinions in the contributions rests entirely on their authors.

14. The author (s) must submit declaration that the paper was not published elsewhere.

15. In case of joint papers, communication will be made with the first author.

16. The University will reserve the copyright of the paper once it is accepted for publication in the Journal. The authors must obtain written parmission from REASP, IUT for publication elsewhere.

Procedure for acceptance of papers and publications :

1. Papers submitted for publication will be referred to the listed reviewers for assessment. However, the editorial board will make initial screening of the papers.

2. After the assessment, the authors may be requested to modify/clarify certain points.

3. Accepted/modifed/corrected papers will be published in the next issue of the Journal.